Journal of Applied Fluid Mechanics, Vol. 15, No. 3, pp. 831-842, 2022.
Available online at www.jafmonline.net, ISSN 1735-3572, EISSN 1735-3645.
https://doi.org/10.47176/jafm.15.03.33238

A DDES Model with Subgrid-scale Eddy Viscosity for Turbulent Flow

P. Ding† and X. Zhou

Academy of Building Energy Efficiency of Guangzhou University, Guangzhou, Guangdong, 510006, China
Guangdong Provincial Key Laboratory of Building Energy Efficiency and Application Technologies, Guangzhou, Guangdong, 510006, China
School of Civil Engineering, Guangzhou University, Guangzhou, Guangdong, 510006, China

†*Corresponding Author Email: tingalan@foxmail.com*

(Received July 29, 2021; accepted January 15, 2022)

ABSTRACT

The original (delayed) detached-eddy simulation ((D)DES), a widely used and efficient hybrid turbulence method, is confronted with some flaws containing grid-induced separation (GIS), log-layer mismatch (LLM), and slow RANS-LES transition. A novel hybrid turbulence model, namely production-limited eddy simulation (PLES), depleting the production through introducing the subarid-scale eddy viscosity is proposed. The simulation data of the zero-pressure gradient boundary layer proves that a good performance in mitigating the GIS issue is obtained from the PLES model. The results of the channel flows reveal that the PLES model has eliminated the LLM of the velocity. A good conformity is given for the backward-facing step flow in the PLES simulation, which proves that the PLES model is validated for complex flow. More turbulent scales in the shear layer are captured by the PLES model, which testifies that the PLES model has a faster RANS/LES switch than the IDDES model. The PLES model has a good performance in predicting the cylinder flow with coarser grid resolution. Due to the new LES mode, the PLES model behaves better than the IDDES model in simulating the cylinder flow. Furthermore, the PLES model allows one to use different LES model in the LES portion for other complex flows.

Keywords: CFD; Turbulence model; DDES model; Subarid-scale eddy viscosity; Production-limited eddy simulation.

1. INTRODUCTION

Turbulent flows are characterized by apparently chaotic and random three-dimensional vortices, which are mathematically induced by the non-linear and high-order terms in the momentum equations. When turbulence is present, chemical reaction, energy dissipation, mixing, heat transfer, and drag may be enhanced. Theoretical analysis, experiments, and numerical simulations are the main approaches for studying turbulent flows. Theoretical analysis for turbulent flows is rarely used and limited to get insight into the mechanism of turbulence due to the complexity of turbulent flows. Experiments may be expensive and complex. Numerical simulations or computations are acceptable alternates due to the fast-developing computing power. Numerical simulations offer information in time and space within the computational domain. Numerical methods for turbulent flows include direct numerical simulation (DNS), large-eddy simulation (LES), and Reynolds-averaged Navier-Stokes (RANS) simulation. Unfortunately, because of high computing expenditure needed in the DNS and LES and low accuracy or performance for predicting massively separated flows in the RANS, the hybrid RANS/LES method that could obtain satisfactory results efficiently has been widely used and studied.

Hybrid RANS/LES models aim to work as RANS models near the walls and switch to LES mode away from the walls or in the flow-detached region. There are many hybrid turbulence models including delayed detached-eddy simulation (DDES) (Gritskevich *et al.* 2012; Shur *et al.* 2008; Spalart *et al.* 2006), partial-averaged Navier-Stokes (Girimaji 2005; Pereira *et al.* 2018), scale-adaptive simulation (Menter and Egorov 2010; Zamiri and Chung 2017) and very large-eddy simulation (Han and Siniša 2013; Speziale 1998) and so on. Hybrid RANS/LES models, especially the DDES models, are broadly applied in different kinds of fields ranging from incipient aeronautical engineering (Liu *et al.* 2018; Qin *et al.* 2015) to chemical (Ding *et al.* 2020; Taghinia *et al.* 2016), mechanical (Lin *et al.* 2018; Zhang *et al.* 2019), and civil (Liu and Niu 2016; Yan and Li 2017) engineering. Then, the accuracy of the DDES model is significant. However, original DES is confronted with some flaws. The DDES model was put forward with a shielding function for mitigating the grid-induced separation (GIS) that results from refining the wall-parallel grids in the initial DES computation. GIS is the result of the modeled-stress depletion (MSD). When the grid spacing is small enough to make the DES limiter work, but not small enough to meet the LES requirement, the MSD happens. Therefore, the shielding function should be used to limit the working of the DES limiter. The other two main issues in the (D)DES models are log-layer mismatch (LLM) and slow RANS-LES transition (Spalart 2008). The LLM issue is the fact that two log layers are misaligned when the DES model is used to simulate the developed channel flows. The slow RANS-LES transition issue is the fact that the original DES on typical grids does not obtain RANS-to-LES switch very quickly in the free shear layer. The LLM and slow RANS-LES transition issues are eliminated by the replacement of the cut-off length scale (Ding *et al.* 2019; Reddy *et al.* 2014) or the grid scale (Shur *et al.* 2015). The replacement of the cut-off length scale reduces the modelled turbulence kinetic energy, then resolves more flow eddies to improve the predicted results. And several dynamic DDES models (He *et al.* 2017; Yin *et al.* 2015) are proposed for improving the prediction of complex flows.

The elaborate literature research reveals that the production term or the dissipation term in the two-equation DDES models is respectively decreased or increased by adding the cut-off length scale, which aims to resolve large or detached eddies. A disadvantage of the DDES model is the fact that it does not allow one to use a given LES model in the LES portion of the flow. Even though the previous researchers have used the SGS eddy viscosity to limit the Reynolds stress (Hassan *et al.* 2013; Walters *et al.* 2013) , this may trigger a serious GIS problem. Then, calculating the Reynolds stress using the SGS eddy viscosity requests a strong shielding function. But there is no report studying this strong shielding function. Therefore, a new DDES model that directly draws lessons from the SGS eddy viscosity is proposed. The new DDES model not only considers the DES issues including the GIS, LLM, and slow RANS-LES transition, but also offers a method to benefit from different SGS eddy viscosity.

Given the above analysis, the main structure of the remaining parts is as follows. A new DDES model based on SGS eddy viscosity named by the production-limited eddy simulation (PLES) is put forward in Section 2. In Section 3, for testing the performance of the PLES model, four cases including zero-pressure gradient boundary layer, channel flows, backward-facing step flow, and cylinder flow are predicted in the paper. Section 4 is the summary and several conclusions of the paper.

2. COMPUTATIONAL DETAILS

2.1 Governing Equations

The governing continuity, momentum and energy equations are as below.

$$\frac{\partial \rho}{\partial t}+\frac{\partial}{\partial x_j}\left(\rho u_j\right)=0 \tag{1}$$

$$\frac{\partial}{\partial t}\left(\rho u_i\right)+\frac{\partial}{\partial x_j}\left(\rho u_i u_j\right)=-\frac{\partial p}{\partial x_i} +\frac{\partial}{\partial x_j}\left[\left(\mu+\mu_t\right)\left(\frac{\partial u_i}{\partial x_j}+\frac{\partial u_j}{\partial x_i}\right)\right] \tag{2}$$

Where u_i is the velocities, and p, ρ, and μ are the pressure, the fluid density, and the viscosity, respectively. The turbulent viscosity μ_t is closed by the turbulence models or the DDES equations.

The underlying RANS model is the BSL k-ω model (Menter 1994) which works as the original k-ω model within the inner boundary layer and the standard k-ε model in the outer region. The modeled transport equations of the turbulence kinetic energy k and the specific dissipation rate ω are as follows.

$$\frac{\partial}{\partial t}(\rho k)+\frac{\partial}{\partial x_i}(\rho u_i k)=P_k-\rho\beta^* k\omega +\frac{\partial}{\partial x_i}\left[\left(\mu+\frac{\mu_t}{\sigma_k}\right)\frac{\partial k}{\partial x_i}\right] \tag{4}$$

$$\frac{\partial}{\partial t}(\rho\omega)+\frac{\partial}{\partial x_i}(\rho u_i\omega)=\alpha\frac{\omega}{k}P_k-\rho\beta\omega^2+ \frac{\partial}{\partial x_i}\left[\left(\mu+\frac{\mu_t}{\sigma_\omega}\right)\frac{\partial\omega}{\partial x_i}\right]+2(1-F)\frac{\rho}{\sigma_{\omega 2}\omega}\frac{\partial k}{\partial x_i}\frac{\partial\omega}{\partial x_i} \tag{5}$$

The production term P_k is calculated as below.

$$P_k=\mu_t S^2,\quad S=\sqrt{2S_{ij}S_{ij}} \qquad S_{ij}=0.5\left(\partial u_i/\partial x_j+\partial u_j/\partial x_i\right) \tag{6}$$

The turbulent viscosity μt has the formula as follows.

$$\mu_t=\rho k/\omega \tag{7}$$

The blending function F, turbulent Prandtl numbers σ_k, σ_ω, and model constants α, β are the same as those in the Ref. (Menter 1994).

2.2 Production-limited Eddy Simulation

For resolving large turbulent eddies, the production term or the dissipation term in the two-equation DDES models is respectively decreased or increased. Here, to utilize the SGS eddy viscosity, the turbulent viscosity is replaced by the SGS eddy viscosity that is always smaller than the RANS turbulent viscosity in the LES region to depletes the production. Then, the production term of the k equation is substituted by the below formula.

$$P_{ples} = f_d P_k + (1.0 - f_d)\mu_{sgs} S^2 = f_d P_k + (1.0 - f_d)\frac{\mu_{sgs}}{\mu_t}\mu_t S^2 = f_d P_k + (1.0 - f_d)\frac{\mu_{sgs}}{\mu_t} P_k \tag{8}$$

Where the shielding function f_d proposed in the improved DDES model (Gritskevich *et al.* 2012) is shown as follows.

$$\begin{aligned} r_1 &= 0.25 - d_w / h_{\max} \\ f_{d1} &= \min\{2\exp(-9r_1^2), 1.0\} \\ r_2 &= \frac{k/\omega}{\kappa^2 d_w^2 \sqrt{0.5(S^2+\Omega^2)}} \\ f_{d2} &= \tanh((C_{d1} r_2)^{C_{d2}}) \\ f_d &= \max(f_{d1}, f_{d2}) \end{aligned} \tag{9}$$

Where Ω, d_w, and h_{max} are the vorticity magnitude, the distance to the nearest wall, and the maximum edge length of the cell, respectively. The constants C_{d1} and C_{d2} respectively have the values of 14.0 and 3.0 (Ding *et al.* 2019), and κ is the von Kármán constant having the value of 0.41. The PLES model works as RANS mode when the shielding function $f_d = 1.0$, otherwise as LES mode.

The new LES mode in the DDES model is limiting the production with the LES SGS eddy viscosity, so the new DDES model is termed by production-limited eddy simulation (PLES). The new LES mode generically combines RANS and LES models, which is suitable to introduce different LES SGS eddy viscosities. With different SGS eddy viscosities, the PLES model could deal with different complex turbulent flows. What is more, due to the low-stress levels enforced by the LES SGS eddy viscosity, the PLES could deplete the modelled turbulence kinetic energy, and give a rapid RANS-LES transition in separating shear layers.

Because of the correct wall asymptotic behavior for wall-bounded flows, the wall-adapting local eddy-viscosity (WALE) model (Nicoud and Ducros 1999)was applied as the SGS eddy viscosity in the PLES model. The WALE turbulent viscosity is calculated by the Eqs. (10-12).

$$\mu_{sgs} = \rho L_s^2 \frac{\left(S_{ij}^d S_{ij}^d\right)^{3/2}}{\left(S_{ij} S_{ij}\right)^{5/2} + \left(S_{ij}^d S_{ij}^d\right)^{5/4}} \tag{10}$$

$$L_s = 0.325 V^{1/3} \tag{11}$$

$$\begin{aligned} S_{ij}^d &= 0.5(g_{ij}^2 + g_{ji}^2) - (1/3)\delta_{ij} g_{kk}^2 \\ g_{ij} &= \partial u_i / \partial x_j \end{aligned} \tag{12}$$

The numerical methods, including the space discretization, the transient formation, the pressure-velocity coupling method, the time steps, and the residuals, are the same as our previous study(Ding *et al.* 2019).

3. RESULTS AND DISCUSSION

A new DDES model based on the SGS eddy viscosity named by the PLES model is put forward in Section 2. For examining the capacity of the PLES model, zero-pressure gradient boundary layer, channel flows, backward-facing step flow, and cylinder flow are simulated and analyzed in the paper. And the simplified version of SST improved-DDES model (hereafter IDDES) (Gritskevich *et al.* 2012) is chosen as the compared model.

3.1 Zero-pressure Gradient Boundary Layer ZPGBL

The ZPGBL simulation is conducted on an ambiguous mesh to investigate the capacity of the DDES models in ameliorating the GIS issue. In the ZPGBL simulation, the streamwise grid spacing before $Re_x = xu_0/v = 5 \times 10^6$ is boundary layer thickness δ_{bl} at $Re_x = 10^7$. The grid spacing after $Re_x = 5 \times 10^6$ and another wall-parallel grid spacing are $0.1\delta_{bl}$.

Figure 1 gives the simulated skin friction coefficient C_f (a) and the maximum turbulent viscosity ratio (b). It shows that the predicted C_f agrees well with the experimental and the BSL results before $Re_x = 6 \times 10^6$. After $Re_x = 6 \times 10^6$, the errors of the C_f by the two hybrid models comparing to the experimental and BSL results become greater and greater. This results from the fact that the LES region becomes larger and larger.

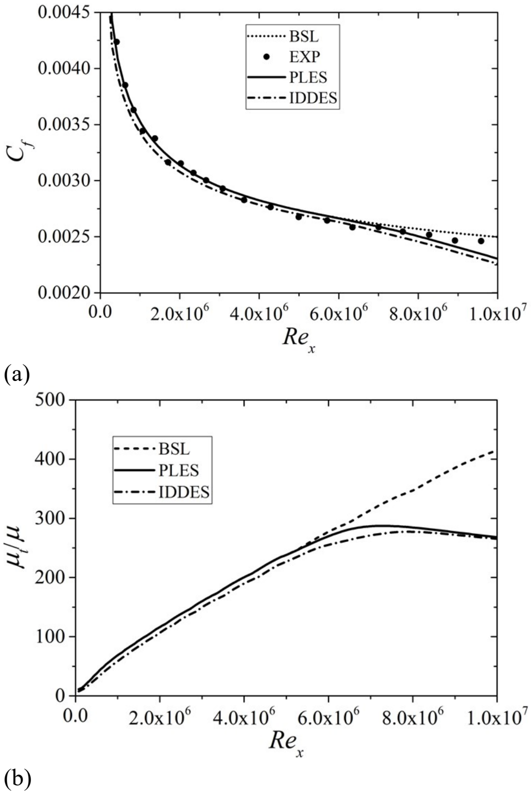

Fig. 1. Skin friction coefficient (a) and maximum turbulent viscosity ratio(b) profiles along the plate.

Figure 1(a) also presents that the predicted C_f by the PLES model is greater than that by the IDDES model, and the maximum error is -1.3% at $Re_x = 10^7$ in contrast with the BSL result. The turbulent viscosity ratios correspondingly exhibit the same profiles presenting in Fig. 1(b). Because of the LES region forming within the boundary layer, the turbulent viscosity is depleted after $Re_x = 6 \times 10^6$. Figure 2 gives the turbulent viscosity ratio at $Re_x = 7.4 \times 10^6$. It shows that the IDDES turbulent viscosity is smaller than the PLES turbulent viscosity, resulting the lager error of C_f.

In summary, the PLES model has a better performance in alleviating the GIS issue comparing with the IDDES model.

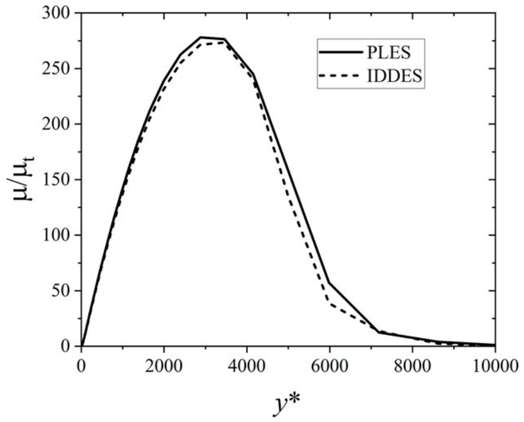

Fig. 2. Turbulent viscosity ratio at *Re_x* = 7.4 × 10⁶.

3.2 Channel Flows

The next case is the plane developed channel flow. This case aims to investigate the LLM issue of the velocity in the PLES simulations. The computational domain, grids, and frictional Re_τ number ($Re_\tau = \delta u_\tau/\nu$, u_τ and δ are the friction velocity and half-height of the channel, respectively) are summarized in Table 1. The first grids near the walls were placed at $y^+ = 1$.

Figure 3 gives the time-averaged streamwise velocity profiles for the channel flow at $Re_\tau = 550$, showing that the predicted profile obtained by the PLES model agrees better with the DNS data (Bernardini *et al.* 2014) comparing with the IDDES model. The key factor is the low-stress levels enforced by the LES SGS eddy viscosity, so the PLES could deplete the modelled turbulence kinetic energy greatly. The PLES model predicts a smaller turbulent viscosity in comparison with the IDDES model in the channel core region, as shown in Fig. 4. It is also important that the PLES model obtains a larger turbulent viscosity in the near-wall region. This is good for resolving more flow scales in the core region and performing good RANS mode near the wall. This is the reason for eliminating the LLM issue.

For the higher Re_τ number Re_τ =2000, whose simulation result is displayed in Fig. 5., satisfactory prediction is given by the PLES model. The predictions of the channel flows at $Re_\tau = 550$ and 2000 prove that the LLM issue is eliminated in the PLES computations.

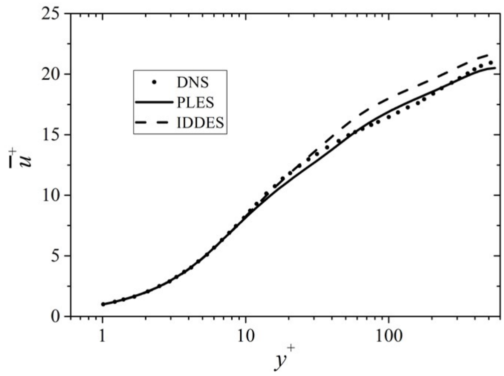

Fig. 3. Time-averaged streamwise velocity profiles for the channel flow at $Re_\tau = 550$.

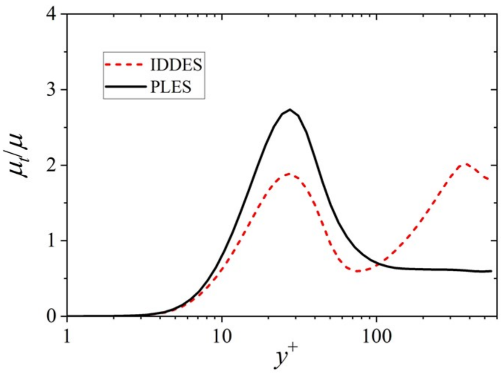

Fig. 4. Turbulent viscosity ratio for the channel flow at $Re_\tau = 550$.

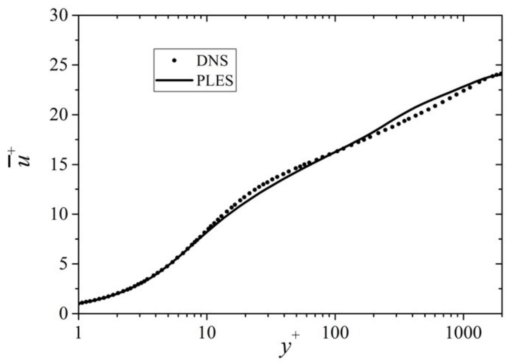

Fig. 5. Time-averaged streamwise velocity profiles for the channel flow at Re_τ =2000.

Table 1 Flow conditions, computational domain, and grid resolution for the channel flows.

Re_τ	Computational domain	Cell number $N_x \times N_y \times N_z$	Δx^+	Δz^+
550	$8\delta \times 2\delta \times 3\delta$	80×100×60	55	27.5
2000	$12\delta \times 2\delta \times 4.5\delta$	80×110×60	300	150

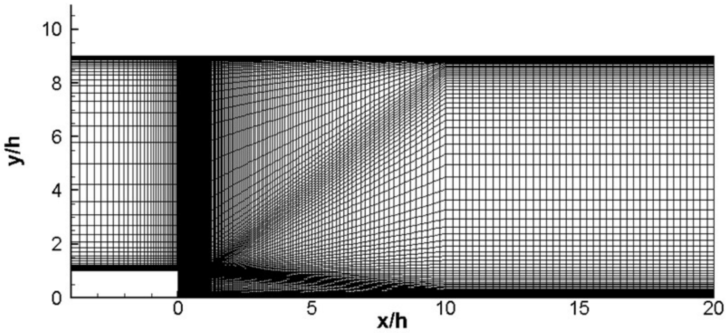

Fig. 6. Grid outline for the BFS flow.

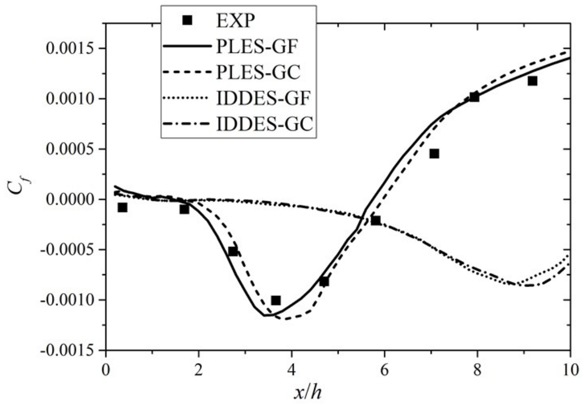

Fig. 7. Skin frictional coefficient profiles along the bottom wall for the BFS flow.

3.3 Backward-facing step flow

In engineering appliances, there appears more complex turbulent flows, such as backward-facing step (BFS) flow. Furthermore, the BFS flow has been a benchmark case for testing the DDES models (Ding *et al.* 2019; Gritskevich *et al.* 2012; Reddy *et al.* 2014; Shur *et al.* 2015). The BFS flow is a good case for the DDES models to examine the slow RANS-LES transition issue. The BFS computational domain contains 24h, 9h, and 3h in the streamwise(x), cross-stream(y), and spanwise(z) directions respectively, and h is the step height. The inlet is located at x/h = -4, and the expansion ratio is 1.125, as shown in Fig. 6. The Re_0 number based on the height of the step and the free velocity u_0 is 37000. The boundary layer thickness is 1.5h. The flow condition is the same as the experiment of Driver and Seegmiller (Driver and Seegmiller 1985) which provides the referenced data.

There are N_{xy}×N_z = 22700 × 30 (GF) or 15630 × 24 (GC) cells discretizing the computational domain. The grids are dense around the step, and the y+ near the walls is about 1~2. The top and bottom walls are set to no-slip wall, and the spanwise direction is periodic. The incoming flow condition is given from a preliminary BSL k-ω RANS computation. The statistical time is about 40 flow-through times, and the statistical results are also averaged in the spanwise direction. The initial effect is removed after 20 flow-through times. The time interval is set to 0.005h/u_0 for keeping the CFL under 2.

Figure 7 provides the skin frictional coefficient profiles C_f along the BFS bottom wall. The C_f profiles obtained from the PLES computations conform to the experimental results, while those in the IDDES computations has significant difference with the experimental results. Meanwhile, there are not great discrepancy between the simulation results on the two grids. The points C_f = 0, which is the locations of the reattachment, given by the PLES model agree well with the experiment. Whereas, the IDDES model overestimates the recirculation zone where C_f < 0.

The time-averaged streamwise velocity profiles at different locations x/h = 2, 4, 6, 8 are drew in Fig. 8. Obviously, the velocity profiles predicted by the PLES model agree better with the experimental data than those predicted by the IDDES model on GC. Especially at locations x/h = 6 and 8, the velocities from the PLES computation and the experiment are positive near the bottom wall, while those form the IDDES computation are negative. This also means that the IDDES model over-predicts the recirculation zone.

The resolved turbulence kinetic energy (r-TKE) and resolved Reynolds shear stress (r-RSS) profiles at different locations on GC are respectively displayed in Figs. 9 and 10. The r-TKE is defined as $0.5(u^{`2}+v^{`2})/u_0^2$ that is the same as the experimental investigation (Driver and Seegmiller 1985). In the prediction of the PLES model, the maximum r-TKE is under-estimated at the most of the locations, and the points of the maximum r-TKE are further from the bottom wall. The maximum r-RSS is over-estimated, and the locations of the maximum r-RSS are higher than experimental results. These errors

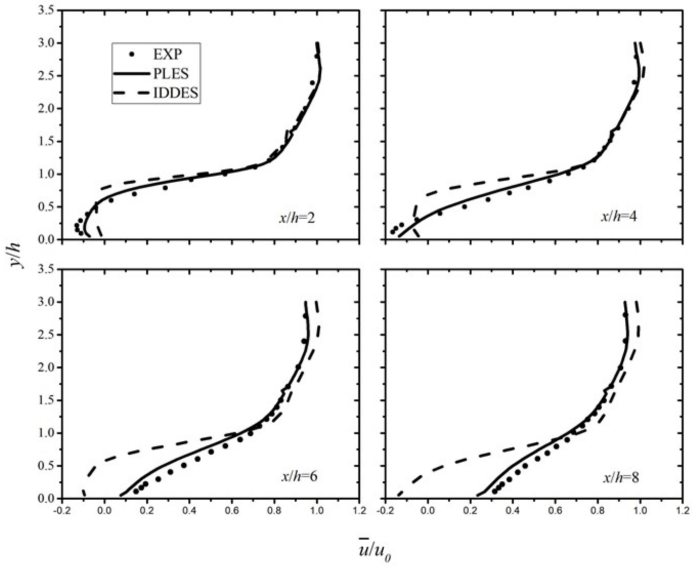

Fig. 8. Time-averaged streamwise velocity profiles at different locations for the BFS flow on GC.

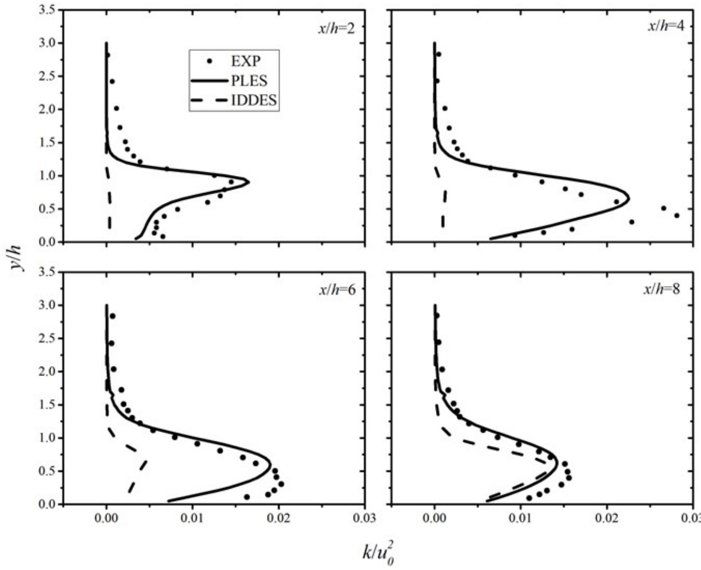

Fig. 9. Resolved turbulence kinetic energy profiles at different locations for the BFS flow on GC.

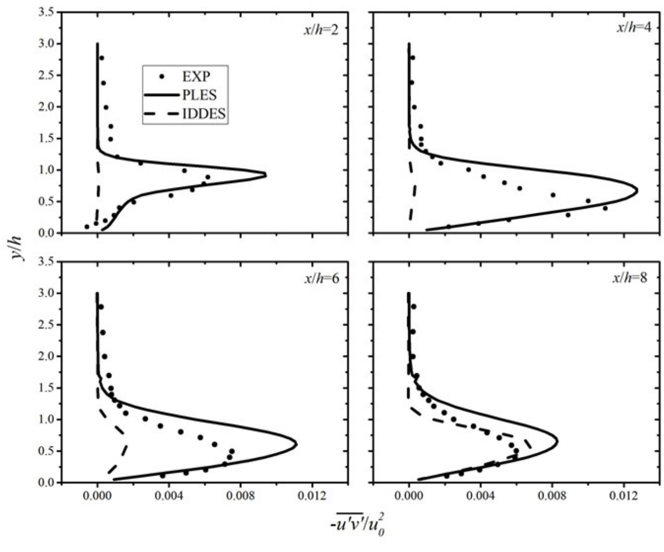

Fig. 10. Resolved Reynolds shear stress profiles at different locations for the BFS flow on GC.

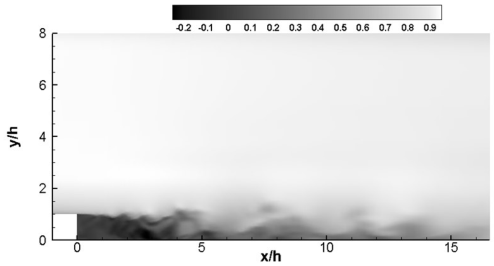

(a) PLES model

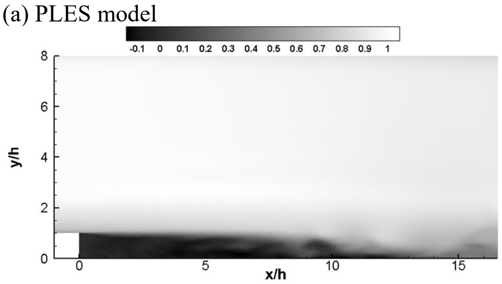

(b) IDDES model

Fig. 11. Contours of the instantaneous streamwise velocity for the BSF on GC.

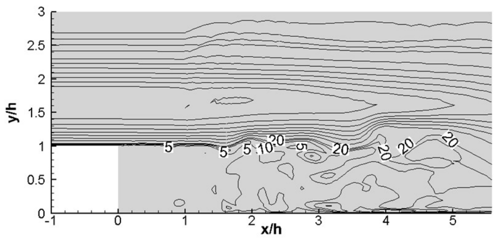

(a) PLES model

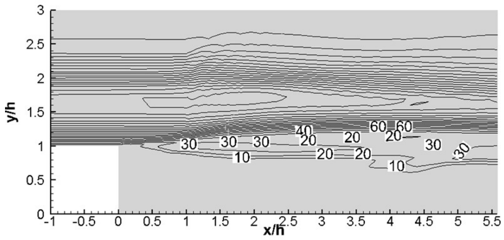

(b) IDDES model

Fig. 12. Lines of instantaneous turbulent viscosity ratio for the BFS flow on GC.

could be removed by refining the grid and applying fluctuating incoming boundary conditions.

Figures 9 and 10 simultaneously shows that the IDDES model gives much smaller r-TKE and r-RSS at all locations except x/h = 8. The instantaneous streamwise velocity for the BSF is provided in Fig. 11. It is evident the PLES model obtains more turbulent eddies due to the KH instability than the IDDES model. This proves that the PLES model gives quicker RANS-LES transition, then unlocks the KH instability after the step more rapidly than the IDDES model.

Figure 12 represents the lines of instantaneous turbulent viscosity ratio obtained by the PLES and IDDES models on GC. Much larger turbulent viscosity is given by the IDDES model in the shear layer, comparing with the PLES results. Then, less turbulent scales are resolved in the IDDES computation. The difference between the PLES model and the IDDES model is the LES mode. The PLES model can deplete the turbulent viscosity and resolve lager scale eddies after the step is due to low-stress levels enforced by the LES SGS eddy viscosity. Therefore, the PLES model can give enough transport of momentum, obtaining reasonable recirculating flow structures. In a word, the PLES model has faster RANS-LES transition than the IDDES model.

3.4 Cylinder flow

For the cylinder flow, the lengths of the streamwise (x), transverse (y), and spanwise (z) directions are respectively 25d, 20d, and πd (d is the diameter), which are shown in Fig. 13, where is the grid outline. Re = $u_0 d/v$ number is 3900. The experimental and LES results from Ref. (Parnaudeau *et al.* 2008) are chosen as the reference data for the evaluation.

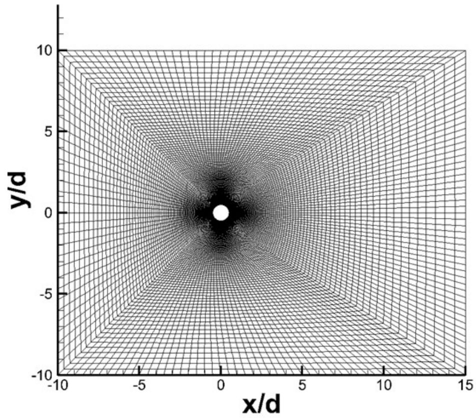

Fig. 13. Grid for the cylinder flow at Re = 3900.

The inlet boundary where uniform velocity u_0 is imposed is located at 10d away from the cylinder center. No-slip wall condition is set at the cylinder surface. The symmetry conditions are used at the lateral walls. The spanwise direction is periodic. The pressure at the outlet boundary is set to zero.

The computational domains, the grid numbers and the grid spacing in the spanwise directions Δz for the cylinder flow are given in Tables 2. Table 2 shows that grid resolution in the spanwise direction used in the computations are coarser than those in the previous studies. The grids are clustered around the cylinder surfaces and the first grids are located at about r^+ =1~2.

The finer grids with $N_{xy}\times Nz$ = 38480×42 cells are used to simulate the cylinder flow in the PLES computations. The time-averaged drag coefficients are 0.99 and 1.00 with $N_{xy}\times Nz$ = 38480×42 and Nz = 24480×32 respectively, and the lengths of the recirculation zones are 1.56 and 1.55 with $N_{xy}\times Nz$ = 38480×42 and Nz = 24480×32 respectively. This shows that refining the gird do not make a significant discrepancy in the PLES computations. Thus, the grid in the Table 2 is used in this paper.

Table 2 Computational domains and grid numbers for the cylinder flow at Re_0 = 3900.

Method	Computational domain	Cell number N_{xy}×N_z	Δz
PLES	Hexahedron 25d×20d×πd	24480×32	0.0981d
IDDES	Hexahedron 25d×20d×πd	24480×32	0.0981d
Jee-DES (Jee and Shariff 2014)	Hexahedron 65d×30d×πd	6000000	–
Luo-SST DES(Luo *et al.* 2014)	Cylinder 60d×0.5πd	37240×30	0.0523d
D`Alessandro-SA IDDES(D'Alessandro *et al.* 2016)	Hexahedron 50d×20d×πd	82400×48	0.0654d
Luo-SST PANS(Luo *et al.* 2014)	Cylinder 60d×0.5πd	37240×30	0.0523d
Parnaudeau-LES(Parnaudeau *et al.* 2008)	Hexahedron 20d×20d×πd	230880×48	0.0654d
Afan-LES(Afgan *et al.* 2011)	Hexahedron 25d×20d×4d	50780×256	0.0156d
Wornom-LES(Wornom *et al.* 2011)	Hexahedron 35d×40d×πd	18000×100	0.0314d
Dong-DNS(Dong *et al.* 2006)	Hexahedron 40d×18d×πd	–×128	0.0245d

Table 3 Comparisons of the global parameters for the cylinder flow at Re_0 = 3900.

Method	θ_{sep}	St	L_r/d	$\overline{C_d}$	C_{drms}	C_{lrms}
PLES	86.4	0.209	1.55	1.00	0.035	0.118
IDDES	88.1	0.209	1.15	1.09	0.064	0.244
Jee-DES(Jee and Shariff 2014)	86.1	0.214	1.44	1.00	–	–
Luo-SST DES(Luo *et al.* 2014)	86.4	0.203	1.46	1.01	–	–
D`Alessandro-SA IDDES(D'Alessandro *et al.* 2016)	87	0.222	1.43	1.02	–	0.146
Luo-SST PANS(Luo *et al.* 2014)	87.3	0.201	1.20	1.06	–	–
Parnaudeau-LES(Parnaudeau *et al.* 2008)	88.0	0.208 ± 0.002	1.56	–	–	–
Afan-LES(Afgan *et al.* 2011)	86.0	0.207	1.49	1.02	0.033	0.137
Wornom-LES(Wornom *et al.* 2011)	89	0.210	1.45	0.99	–	0.110
Dong-DNS(Dong *et al.* 2006)	–	0.203	1.59	–	–	–
Parnaudeau-EXP[30]	88.0	0.208	1.51	–	–	–
Lourenco-EXP(Lourenco 1994)	85 ± 2	0.215 ± 0.005	1.33 ± 0.2	0.98 ± 0.05	–	–

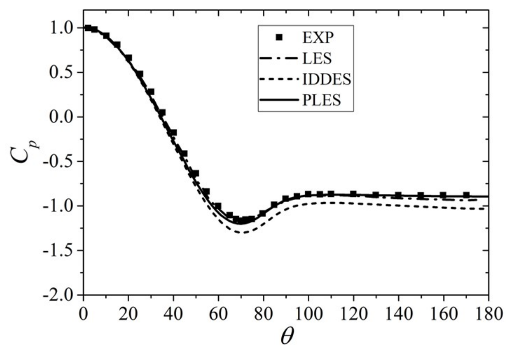

Fig. 14. Profiles of the pressure coefficient C_p along the circular cylinder.

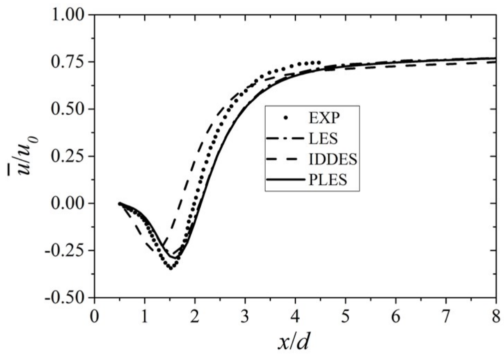

Fig. 15. Profiles of the time-averaged streamwise velocity at the cylinder wake y/d = 0.

Figure 14 shows the profiles of the pressure coefficient C_p along the circular cylinder. For C_p, the PLES model gives good agreement with the experimental and the LES results, while the IDDES model under-predicts C_p on the leeward side. The profiles of the time-averaged streamwise velocity at the cylinder wake y/d = 0 are shown in Fig. 15. It shows that the PLES model gives a good correlation with the experimental and the LES data. While, the profile of the predicted streamwise velocity from the IDDES simulation shifts upwards and moves to the cylinder having a big discrepancy with the experimental data.

Table 3 summaries the comparisons of the global parameters for the cylinder flow at Re_0 = 3900. It is noted that the flow separation angles θ_{sep} predicted by all the models are less than 90° and conform well to the experimental data, and their differences are little. All the models except for the D`Alessandro-SA IDDES model have good performance in estimating the Strouhal (St) number. The length of the recirculation zone L_r/d is defined as the distance between the location of the zero time-averaged streamwise velocity at y/d = 0 and the cylinder surface. It is noted that the IDDES model greatly under-estimates L_r/d comparing with the experimental and the LES results. While, L_r/d predicted by the PLES model agrees well with the reference data. For the time-averaged drag coefficient $\overline{C_d}$, the IDDES model obtains greater value than the other models and the experiment. The PLES model obtains satisfactory result of the drag coefficient. Comparing with the root mean square (RMS) drag coefficient C_{drms} and the RMS lift coefficient C_{lrms} predicted by the Afan-LES computation, the IDDES model predicts values double those of other methods, while the PLES model gives the satisfactory results.

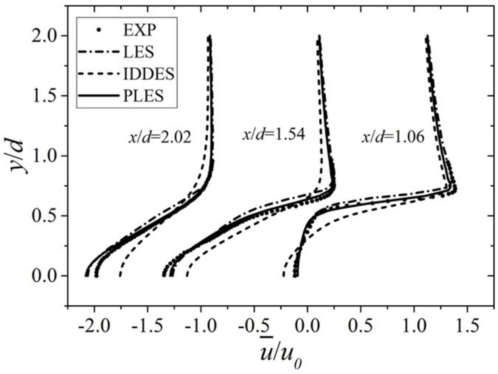

(a)

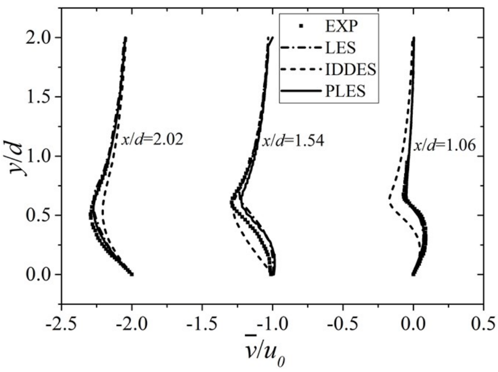

(b)

Fig. 16. Profiles of the time-averaged streamwise velocity (a) and the time-averaged transverse velocity (b) for the cylinder flow.

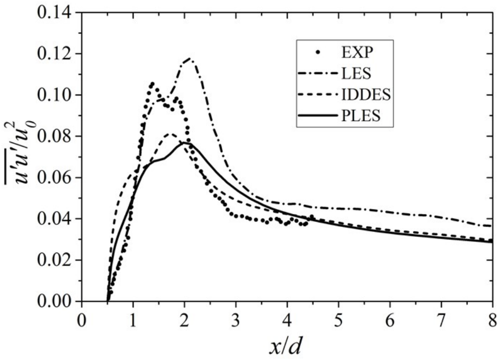

Fig. 17. Profiles of the resolved streamwise Reynolds normal stress.

Figure 16 gives the profiles of the time-averaged streamwise velocity (a) and the time-averaged transverse velocity (b) for the cylinder flow. The predicted streamwise velocity from the PLES simulation occurs a U-shape profile in the near-cylinder wake x/d = 1.06 and a V-shape further downstream x/d = 1.54 and 2.02, which is consistent with the experimental data. However, the IDDES model predicts a V-shape streamwise velocity profile in the near-cylinder wake x/d = 1.06 and 1.54 and a U-shape further downstream x/d = 2.02, which differs greatly from the experimental data. Concerning the transverse velocity, the PLES model gives the well-matched profiles comparing with the experimental data, while the IDDES model makes a significant discrepancy.

Figure 17 presents the profiles of the resolved streamwise normal stress (r-sRNS) at the cylinder wake y/d = 0. It shows that the experimental result has two peaks, while the LES, the IDDES, and the PLES results have only one peak. What is more, the location of the peak predicted by the IDDES model moves more closely to the cylinder than that predicted by the PLES model.

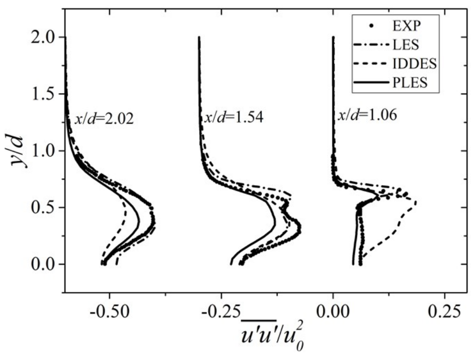

(a)

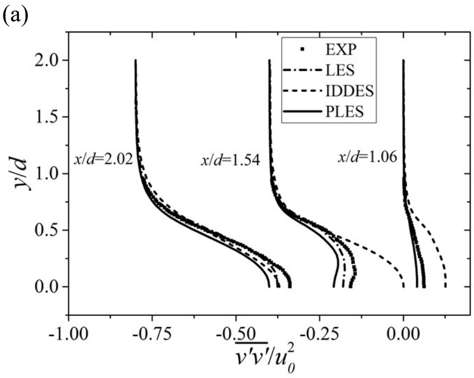

(b)

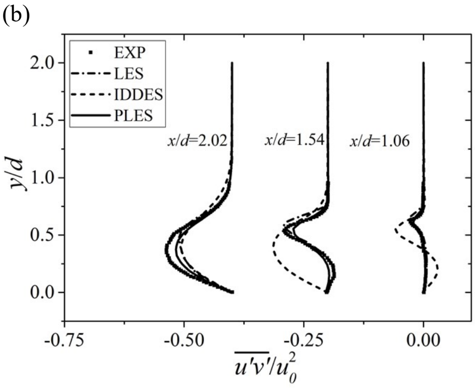

(c)

Fig. 18. Profiles of the resolved streamwise Reynolds normal stress (a), the resolved transverse Reynolds normal stress (b), and the resolved Reynolds shear stress (c) for the cylinder flow.

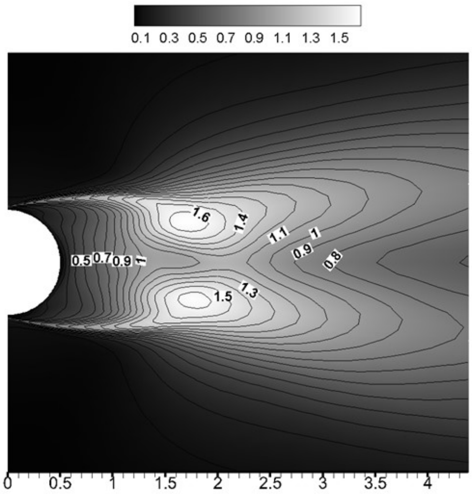

(a) PLES model

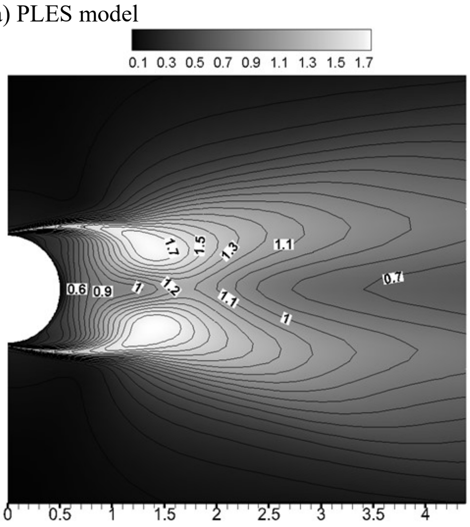

(b) IDDES model

Fig. 19. Contours of the resolved streamwise Reynolds normal stress for the cylinder flow.

The profiles of the resolved streamwise Reynolds normal stress (r-sRNS) (a), the resolved transverse Reynolds normal stress (r-tRNS) (b), and the resolved Reynolds shear stress (r-RSS) (c) for the cylinder flow are shown in Fig. 18. It indicates that the PLES model under-predicts the r-sRNS and the r-tRNS, which is because part of the RNS is modeled. The significant over-predictions of the r-sRNS and the r-tRNS in the DDES simulation occur at x/d = 1.06 and x/d = 1.06 &1.54 respectively. Figure 16(c) shows the r-RSS given by the PLES model matches well with the experimental and the LES results. Nonetheless, the IDDES model gives a large difference with the reference data.

Analyzing Fig. 18, it is found that the distributions of the variables obtained from the IDDES model at x/d = 1.06 and 1.54 are respectively similar to those from the PLES and experimental results at x/d = 1.54 and 2.02. This reveals that the length of the recirculation zone is under-estimated and the location of the shear layer instability is predicted earlier by the IDDES model. Figure 19 displays the contours of the resolved streamwise Reynolds normal stress for the cylinder flow. It is gotten that the location of the maximum r-sRNS is estimated more closely to the cylinder by the DDES model than that by the PLES model. The locations of the maximum r-sRNS in the PLES and the IDDES computations are predicted at x/h = 1.75 and 1.35 respectively. This reveals that the shear layer instability unlocks more closely to the cylinder in the IDDES prediction. The contours of the r-sRNS also reveal that the length of the recirculation zone is shorter in the IDDES computation than that in the PLES computation.

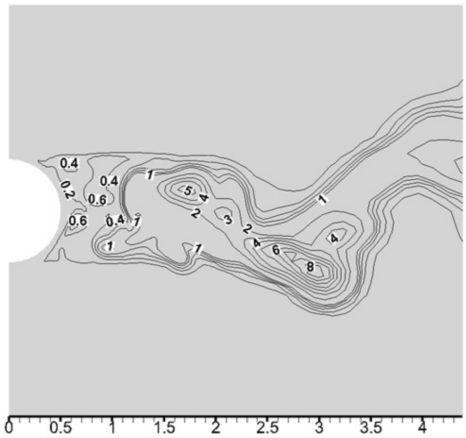

(a) PLES model

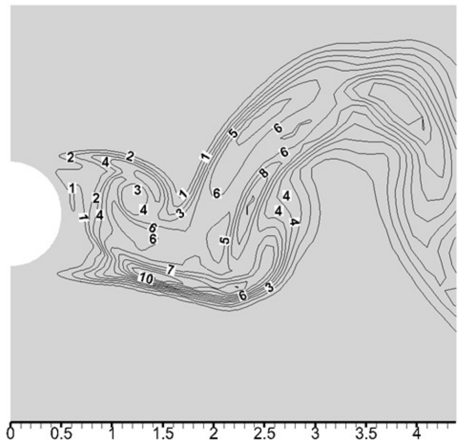

(b) IDDES model

Fig. 20. Contours of the turbulent viscosity ratio for the cylinder flow.

The large discrepancy of the performance between the PLES model and the IDDES model results from the different LES mode as analyzed in the BFS flow. Therefore, comparing with the PLES model, the IDDES model over-resolves the turbulent viscosity in the wake region, which is shown in Fig. 20. Figure 20 shows that the DDES turbulent viscosity is much larger than the PLES turbulent viscosity near the cylinder where the turbulent viscosity should be small. This leads to the early appearance of the shear layer instability and the short recirculation zone. Nevertheless, the PLES model computes reasonable flow structures and turbulent viscosity in the wake resulting from its LES mode.

In summary, on the one hand, the PLES model has a good performance in predicting the cylinder flow with coarse grid resolution. On the other hand, due to the new LES mode, the PLES model performs better in predicting the cylinder flow comparing with the IDDES model on the used grid resolution in this study.

4. CONCLUSIONS

A new delayed detached-eddy simulation (DDES) model with the sub-grid scale (SGS) eddy viscosity limiting the production named by production-limited eddy simulation (PLES) model is put forward. For testing the capacity of the PLES model, zero-pressure gradient boundary layer (ZPGBL), channel flows, backward-facing step flow, and cylinder flow are simulated and analyzed. The conclusions are as below.

(1) To mitigate the grid-induced separation (GIS) issue, the shielding function is used to enlarge the RANS region. The ZPGBL simulation shows that the PLES model with the shielding function has a little better performance in easing the GIS issue comparing with the IDDES model. The predicted velocity of the channel flows conforms well to the DNS data and has only one log-layer region. This reveals that the PLES model has eliminated the log-layer mismatch issue of the velocity.

(2) Since low-stress levels are enforced by the LES SGS eddy viscosity, more turbulent scales in the shear layer are captured by the PLES model. As a result, the PLES model can give enough transport of momentum, obtaining reasonable recirculating flow structures. A good agreement is obtained for backward-facing step flow in the PLES simulation, which proves that the PLES model is validated for complex flow. This also testifies that the PLES model has a faster RANS/LES switch than the IDDES model.

(3) Comparing with the IDDES model, the PLES model resolves the smaller turbulent viscosity in the wake region due to the new LES mode. This leads to the accurate appearance of the shear layer instability and the reasonable recirculation zone. And the simulation results of the first and second orders quantities prove that the PLES model behaves better than the IDDES model in simulating the cylinder flow.

It can be concluded that the PLES model not only solves the DES issues but also efficiently predicts complicated flows. And a method for using different SGS eddy viscosity in the hybrid model is offered. What is more, it should test other SGS eddy viscosities in the PLES model for more complex turbulent flows in the future.

ACKNOWLEDGEMENTS

This work is supported by the National Natural Science Foundation of China (Grant No. 52078146) and the Key Project of Basic Research and Applied Basic Research in Universities of Guangdong Province (Grant No. 2018KZDXM050).

REFERENCES

Afgan, I., Y. Kahil, S. Benhamadouche and P. Sagaut (2011). Large eddy simulation of the flow around single and two side-by-side cylinders at subcritical Reynolds numbers. *Physics of Fluids* 23(7), 075101.

Bernardini, M., S. Pirozzoli and P. Orlandi (2014). Velocity statistics in turbulent channel flow up to Re=4000. *Journal of Fluid Mechanics* 742, 171-191.

D'Alessandro, V., S. Montelpare and R. Ricci (2016). Detached–eddy simulations of the flow over a cylinder at Re = 3900 using OpenFOAM. *Computers & Fluids* 136, 152-169.

Ding, P., S. Wang and K. Chen (2019). Production-limited delayed detached eddy simulation of turbulent flow and heat transfer. *Canadian Journal of Chemical Engineering* 97(7), 2146-2156.

Ding, P., S. Wang and K. Chen (2020). Numerical study on turbulent mixed convection in a vertical plane channel using hybrid RANS/LES and LES models. *Chinese Journal of Chemical Engineering* 28(1), 1-8.

Dong, S., G. E. Karniadakis, A. Ekmekci and D. Rockwell (2006). A combined direct numerical simulation–particle image velocimetry study of the turbulent near wake. *Journal of Fluid Mechanics* 569, 185-207.

Driver, D. M. and H. L. Seegmiller (1985). Features of a reattaching turbulent shear layer in divergent channelflow. *AIAA Journal* 23(2), 163-171.

Girimaji, S. S. (2005). Partially-Averaged Navier-Stokes Model for Turbulence: A Reynolds-Averaged Navier-Stokes to Direct Numerical Simulation Bridging Method. *Journal of Applied Mechanics* 73(3), 413-421.

Gritskevich, M. S., A. V. Garbaruk, J. Schütze and F. R. Menter (2012). Development of DDES and IDDES Formulations for the k-ω Shear Stress Transport Model. *Flow, Turbulence and Combustion* 88(3), 431-449.

Han, X. and K. Siniša (2013). An efficient very large eddy simulation model for simulation of turbulent flow. *International Journal for Numerical Methods in Fluids* 71(11), 1341–1360.

Hassan, E., J. Boles, H. Aono, D. Davis and W. Shyy (2013). Supersonic jet and crossflow interaction: Computational modeling. *Progress in Aerospace Sciences* 57, 1-24.

He, C., Y. Liu and S. Yavuzkurt (2017). A dynamic delayed detached-eddy simulation model for turbulent flows. *Computers & Fluids* 146, 174-189.

Jee, S. and K. Shariff (2014). Detached-eddy simulation based on the v2-f model. *International Journal of Heat and Fluid Flow* 46, 84-101.

Lin, D., X. R. Su and X. Yuan (2018). DDES Analysis of the Wake Vortex Related Unsteadiness and Losses in the Environment of a High-Pressure Turbine Stage. *Journal of Turbomachinery-Transactions of the Asme* 140(4), 041001.

Liu, J. and J. Niu. (2016). CFD simulation of the wind environment around an isolated high-rise building: An evaluation of SRANS, LES and DES models. *Building and Environment* 96, 91-106.

Liu, J., K. Luo, H. Sun, Y. Huang, Z. Liu and Z. Xiao (2018). Dynamic response of vortex breakdown flows to a pitching double-delta wing. *Aerospace Science and Technology* 72, 564-577.

Lourenco, L. M. (1994). Characteristics of the plate turbulent near wake of a circular cylinder. A particle image velocimetry study. *In Unpublished, results taken from Beaudan and Moin*.

Luo, D., C. Yan, H. Liu and R. Zhao (2014). Comparative assessment of PANS and DES for simulation of flow past a circular cylinder. *Journal of Wind Engineering and Industrial Aerodynamics* 134, 65-77.

Menter, F. R. (1994). Two-equation eddy-viscosity turbulence models for engineering applications. *AIAA Journal* 32(8), 1598-1605.

Menter, F. R. and Y. Egorov. (2010). The Scale-Adaptive Simulation Method for Unsteady Turbulent Flow Predictions. Part 1: Theory and Model Description. *Flow, Turbulence and Combustion* 85(1), 113-138.

Nicoud, F. and F. Ducros (1999). Subgrid-Scale Stress Modelling Based on the Square of the Velocity Gradient Tensor. *Flow, Turbulence and Combustion* 62(3), 183-200.

Parnaudeau, P., J. Carlier, D. Heitz and E. Lamballais (2008). Experimental and numerical studies of the flow over a circular cylinder at Reynolds number 3900. *Physics of Fluids* 20(8), 085101.

Pereira, F. S., G. Vaz, L. Eça and S. S. Girimaji (2018). Simulation of the flow around a circular cylinder at Re=3900 with Partially-Averaged Navier-Stokes equations. *International Journal of Heat and Fluid Flow* 69, 234-246.

Qin, Y., Q. Qu, P. Liu, Y. Tian and Z. Lu (2015). DDES study of the aerodynamic forces and flow physics of a delta wing in static ground effect. *Aerospace Science and Technology* 43, 423-436.

Reddy, K. R., J. A. Ryon and P. A. Durbin (2014). A DDES model with a Smagorinsky-type eddy viscosity formulation and log-layer mismatch correction. *International Journal of Heat and Fluid Flow* 50, 103-113.

Shur, M. L., P. R. Spalart, M. K. Strelets and A. K. Travin (2008). A hybrid RANS-LES approach with delayed-DES and wall-modelled LES capabilities. *International Journal of Heat and Fluid Flow* 29(6), 1638-1649.

Shur, M. L., P. R. Spalart, M. K. Strelets and A. K. Travin (2015). An Enhanced Version of DES with Rapid Transition from RANS to LES in Separated Flows. *Flow, Turbulence and Combustion* 95(4), 709-737.

Spalart, P. R. (2008). Detached-Eddy Simulation. *Annual Review of Fluid Mechanics* 41(1), 181-202.

Spalart, P. R., S. Deck, M. L. Shur, K. D. Squires, M. K. Strelets and A. Travin (2006). A New Version of Detached-eddy Simulation, Resistant to Ambiguous Grid Densities. *Theoretical and Computational Fluid Dynamics* 20(3), 181.

Speziale, C. G. (1998). Turbulence Modeling for Time-Dependent RANS and VLES: A Review. *AIAA Journal* 36(2), 173-184.

Taghinia, J., M. Rahman, T. K. T. Tse and T. Siikonen (2016). CFD modeling of homogenizer valve: A comparative study. *Chemical Engineering Research and Design* 106, 327-336.

Walters, D. K., S. Bhushan, M. F. Alam and D. S. Thompson (2013). Investigation of a Dynamic Hybrid RANS/LES Modelling Methodology for Finite-Volume CFD Simulations. *Flow, Turbulence and Combustion* 91(3), 643-667.

Wornom, S., H. Ouvrard, M. V. Salvetti, B. Koobus and A. Dervieux (2011). Variational multiscale large-eddy simulations of the flow past a circular cylinder: Reynolds number effects. *Computers & Fluids* 47(1), 44-50.

Yan, B. W. and Q. S. Li. (2017). Detached-eddy and large-eddy simulations of wind effects on a high-rise structure. *Computers & Fluids* 150, 74-83.

Yin, Z., K. R. Reddy and P. A. Durbin (2015). On the dynamic computation of the model constant in delayed detached eddy simulation. *Physics of Fluids* 27(2), 025105.

Zamiri, A. and J. T. Chung (2017). Ability of URANS approach in prediction of unsteady turbulent flows in an unbaffled stirred tank. *International Journal of Mechanical Sciences* 133, 178-187.

Zhang, N., X. Liu, B. Gao and B. Xia (2019). DDES analysis of the unsteady wake flow and its evolution of a centrifugal pump. *Renewable Energy* 141, 570-582.